ISIJ International, Vol. 45 (2005), No. 11, pp. 1597–1606

Solid Inclusion Transfer at a Steel–Slag Interface with Focus on Tundish Conditions

J. STRANDH, K. NAKAJIMA, R. ERIKSSON and P. JÖNSSON

Division of Applied Process Metallurgy, KTH, SE-100 44 Stockholm, Sweden.

(*Received on April 25, 2005; accepted on July 7, 2005*)

The separation of non-metallic inclusions from the steel to the slag phase in the ladle during secondary steel making operations and in the tundish and mold during casting is very crucial to the production of clean steel. In this work a theoretical study of the separation of solid inclusions, alumina and others, at the steel–slag interface applied to the actual conditions in the tundish has been carried out. The theoretical model is based on the equation of motion with the following forces acting on an inclusion as it tries to cross the interface between the metal and the slag; buoyant, added mass, rebound and drag force. A sensitivity analysis study was carried out in order to clarify which of the parameters in the model that had the largest influence on the inclusion displacement. The results showed that the interfacial tensions (σ_{MI}, σ_{IS}, σ_{MS}) and the slag viscosity (μ_S) have the largest influence on the predicted displacement. It was also concluded that the overall wettability should be positive and that the slag viscosity should be as low as possible to obtain the most favorable conditions for inclusion transfer at the steel–slag interface.

KEY WORDS: modeling; inclusions; steel; slag; transfer; physical properties and tundish.

1. Introduction

Today, the tundish is regarded to be an important metallurgical reactor and not only an intermediate steel buffering vessel between the ladle and the caster. However, if the tundish is used in the right way it can also be utilized to separate non-metallic inclusions present in the steel. If the desire of the steelmaker is to use the tundish as an important metallurgical tool it is essential to have a good control and a deep understanding of all aspects of the tundish operation, including for example, throughput rate of steel, chemical composition and amount of tundish slag, temperature of the steel and suitable measures to avoid ladle slag carry over. In order to be able to control and affect the separation of non-metallic inclusions from the steel to the tundish covering flux it is important to understand the mechanisms involved in the transfer of inclusions across the interface between the steel and the tundish covering slag.

The separation of non-metallic inclusions at the interface between the steel and the slag in the tundish as well as in the ladle and mold is to a great extent controlled by interfacial phenomena in the steel–slag-inclusion system. It is therefore important to know how, the interfacial properties governing the inclusion separation from the liquid steel can be controlled towards a desired result. Great care must be observed since interfacial conditions that appear to have a positive effect on the inclusions transfer across the interface might have negative consequences on other aspects. The following criteria have to be fulfilled in order to achieve optimal inclusion removal at a steel–slag interface: a) Separation of the inclusions to the slag, b) High dissolution of the inclusions, and c) Prevention of reoxidation.

In this work a mathematical model for the separation of inclusions from the steel to the slag, developed by Nakajima and Okamura,[1] has been used to study the inclusion transfer when the inclusion has reached the steel–slag interface. It is assumed that the inclusion has been carried to the interface by the flow field and that it reaches the interface with the terminal velocity determined by the buoyancy force and the fluid dynamic drag. The model predicts two modes of inclusion transfer, one where a steel film is formed between the inclusion and the slag as the inclusion is crossing the interface and one without the formation of the steel film.

The main aim of this work has been to study how solid inclusions, alumina and others, behave at a steel–slag interface with focus on the tundish process. Here, it was seen important to first carry out a parameter study to determine which of the model variables that have the largest influence on the predicted inclusion displacement at the interface. In addition, the available literature data and models available for physical property data, which are necessary to use when modeling inclusion transfer at the steel–slag interface were studied. Finally, it was important to exemplify how the model can be used to study inclusion transfer for industrial conditions.

Firstly, the mathematical model describing the behavior of a solid spherical non-metallic inclusion at the steel–slag interface is outlined. This is followed by a brief description of the conditions at the two steel plants from which data have been taken. Thereafter, the results are presented and discussed.

2. Mathematical Model of Particle Behavior across the Steel–Slag Interface

A mathematical model of inclusion transfer at a steel–slag interface has been developed. The original description of the mathematical model has previously been presented at a conference by Nakajima and Okamura.[1] The mathematical model proposes two types of inclusion transfer situations when the solid spherical inclusions cross the steel–slag interface. The two situations, with and without a steel

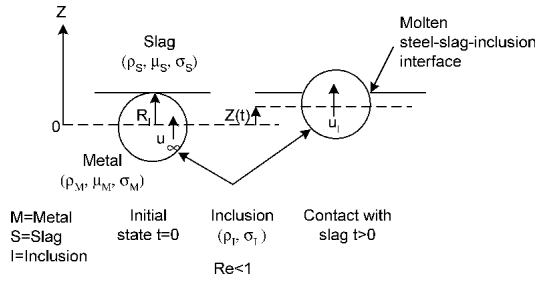

Fig. 1. Schematic diagram describing the inclusion transfer to the slag without the film formation between the inclusion and the slag.

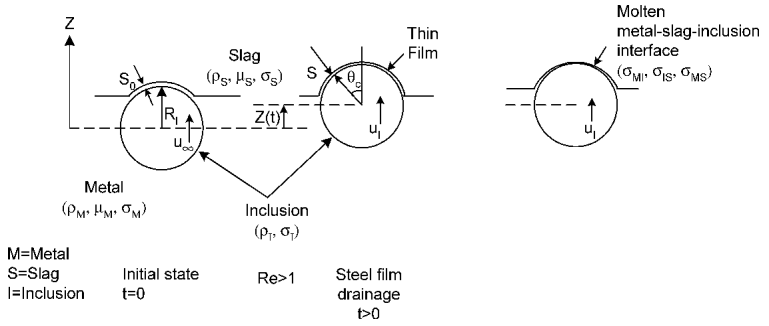

Fig. 2. Schematic diagram describing the inclusion transfer to the slag with the formation of a thin steel film between the inclusion and the slag.

film between the inclusion and the interface are schematically outlined in **Figs. 1** and **2**, respectively. In the case where Re≧1, the inclusions are always accompanied with steel around them, so that the steel is not pushed away rapidly. Thus, a thin steel film will still exist between the inclusion and the interface when the inclusion reaches the steel–slag interface. If Re<1, no steel film will be formed and the inclusion will be in direct contact with the slag at the interface.

2.1. Assumptions

The following general assumptions are made in the modeling of the inclusion transfer across the steel–slag interface:

- The inclusion is solid and spherical with constant volume.
- No chemical reactions between the phases.
- All fluids are incompressible and isothermal.
- The slag phase is assumed to be liquid.
- The interface between steel and slag is flat.
- The inclusion transfer depends on the buoyancy, added mass, drag and rebound force.
- The interfacial tension is uniform along the interface.

When the inclusion has traveled one diameter from its original position, it is assumed to be completely absorbed into the slag.

Note, that for the case with a steel film, some additional assumptions are needed. These assumptions will be outlined in Sec. 2.4.

2.2. General Equations

At a start of a calculation, the center of the inclusion is defined as the initial position, $Z=0$, situated one inclusion radius from the interface, as illustrated in Figs. 1 and 2. Thus, the surface of the inclusion is in contact with the interface, $Z=R_I$. Although the inclusion is generally carried by the steel flow to the interface, here it is assumed to have an initial velocity equal to its terminal velocity, which is given by

$$u_\infty = \frac{2}{9} R_I^2 (\rho_M - \rho_I) \frac{g}{\mu_M} \quad \text{.....(1)}$$

where ρ_M and ρ_I is the density of the metal and the inclusion respectively, μ_M is the viscosity of the metal phase, g is the gravitational acceleration and R_I is the inclusion radius.

Four different forces are assumed to act on the inclusion as it approaches the steel–slag interface: the buoyant force (F_b), the rebound force (F_r), the added mass force (F_f), and the drag force (F_d). Thus, the following equation of motion over the system can be formulated

$$\frac{4}{3}\pi R_I^3 \rho_I \frac{d^2 Z}{dt^2} + F_f = F_b - F_d - F_r \quad \text{.....(2)}$$

Alhough the buoyant force always acts upwards, the rebound force, added mass force and the drag force can act both upwards and downwards depending on the behavior of the inclusion at the interface. In the following description, the equations will be expressed in dimensionless variables, since it will make them easier to solve. In dimensionless variables, it is assumed that the inclusion is completely transferred to the slag when the dimensionless displacement is equal to 2 ($Z^*=2$). The displacement, Z, time, t, and velocity, dZ/dt, can be made dimensionless by multiplying with $1/R_I$, $\sqrt{g/R_I}$ and $1/\sqrt{g/R_I}$ respectively.

2.3. Inclusion Transport without a Steel Film

The displacement of the inclusion from its original location will be derived from the equation of motion, Eq. (2). For inclusion transport when no steel film is formed, the buoyant force, positive in the upward direction, is described by

$$F_b = \frac{4}{3}\pi R_I^3 g(\rho_S \cdot A(Z^*) - \rho_I) \quad \text{.....(3)}$$

where ρ_S is the density of the slag and $A(Z^*)$ is defined as

$$A(Z^*) = \frac{1}{4}\left(\frac{\rho_M}{\rho_S} - 1\right) Z^{*3} - \frac{3}{4}\left(\frac{\rho_M}{\rho_S} - 1\right) Z^{*2} + \frac{\rho_M}{\rho_S} \quad \text{.....(4)}$$

The added mass force, positive in the downward direction, is given by

$$F_f = \frac{2}{3}\pi R_I^3 \rho_S \cdot A(Z^*) \cdot g \frac{d^2 Z^*}{dt^{*2}} \quad \text{.....(5)}$$

The rebound force, positive in the downward direction, is expressed as

$$F_r = 2\pi R_I \sigma_{MS} B(Z^*) \quad \text{.....(6)}$$

where σ_{MS} is the interfacial tension between the metal and the slag phase and is $B(Z^*)$ defined as

$$B(Z^*) = Z^* - 1 - \cos\theta_{IMS} \quad \text{.....(7)}$$

where $\cos\theta_{IMS}$ is the overall wettability, which is defined as

$$\cos\theta_{IMS} = \frac{\sigma_{IM} - \sigma_{IS}}{\sigma_{MS}} \quad \text{.....(8)}$$

where σ_{IM} and σ_{IS} is the interfacial tension between the inclusion and metal and inclusion and slag respectively. If $\cos\theta_{IMS}<0$ the liquid steel is said to wet the solid inclusion, and if $\cos\theta_{IMS}>0°$ the steel is said to be non-wetting.

Finally, the drag force acting on the inclusion, positive in the downward direction, is given by

$$F_d = 6\pi R_I \mu_S \cdot C(Z^*) \cdot \sqrt{R_I g}\, \frac{dZ^*}{dt^*} \quad \text{.....(9)}$$

where μ_S is the viscosity of the slag and $C(Z^*)$ is defined as

$$C(Z^*) = \left(\frac{\mu_M}{\mu_S} - 1\right) Z^{*2} - 2\left(\frac{\mu_M}{\mu_S} - 1\right) Z^* + \frac{\mu_M}{\mu_S} \quad \text{...(10)}$$

If the expressions for the buoyant force (Eq. (3)), added mass force (Eq. (5)), rebound force (Eq. (6)) and drag force (Eq. (9)) are inserted into the equation of motion (Eq. (2)), the dimensionless displacement of the inclusion from its initial position will be expressed as follows

$$\frac{d^2 Z^*}{dt^{*2}} = 2\,\frac{\rho_S \cdot A(Z^*) - \rho_I}{\rho_S \cdot A(Z^*) + 2\rho_I} - 3 \cdot D(Z^*) \cdot B(Z^*) - \frac{9}{E(Z^*)} \cdot C(Z^*) \cdot \frac{dZ^*}{dt^*} \quad \text{.....(11)}$$

where $D(Z^*)$ and $E(Z^*)$ are given as

$$D(Z^*) = \frac{\sigma_{MS}}{R_I^2 (\rho_S \cdot A(Z^*) + 2\rho_I) g} \quad \text{.....(12)}$$

$$E(Z^*) = \frac{\sqrt{R_I^3 g}\,(\rho_S \cdot A(Z^*) + 2\rho_I)}{\mu_S} \quad \text{.....(13)}$$

By solving Eq. (11) numerically, the displacement of the inclusion from its initial position as a function of time can be obtained.

2.4. Inclusion Transport with a Steel Film

As mentioned earlier, for a situation where Re≥1 a steel film is formed between the rising inclusion and the slag interface. This case requires some additional assumptions to those given in Sec. 2.1. More specifically, the steel film is assumed to be uniform along the surface of the inclusion and also very thin. It is also assumed that the following stream function in spherical coordinates can be used to describe the flow around the inclusion

$$\psi = \frac{1}{2}\frac{dZ}{dt}\left(-\frac{3}{2} r R_I + \frac{1}{2}\frac{R_I^3}{r}\right)\sin^2\theta \quad \text{.....(14)}$$

where r is the distance in the r-direction from the center of the inclusion. A schematic figure of the streamlines around a moving sphere in a liquid at rest is seen in **Fig. 3**. This stream function is valid when $r \geq R_I$ and $0 \leq \theta \leq \pi$.

Inclusions are normally relatively small, and as a result the deformation of the interface is small. Therefore, the slag pressure, P_S, is approximately equal to the metal pressure, P_M. Together with Eq. (14), the continuity of normal stress across the steel film–slag interface can be expressed as:

$$P_F - P_S \cong P_F - P_M = \frac{2\sigma_{MS}}{R_I + S} + \frac{dZ}{dt}\, 2\mu_S\, \frac{3}{2}\left(\frac{1}{R_I + 2S} - \frac{1}{R_I + 4S}\right)\cos\theta \quad \text{.....(15)}$$

where P_F is the steel film pressure and S is the steel film thickness.

The rebound force is obtained by integrating Eq. (15) as follows

$$F_r = \int_0^{\theta_C} (P_F - P_M)\cos\theta \cdot 2\pi R_I \sin\theta \cdot R_I d\theta$$

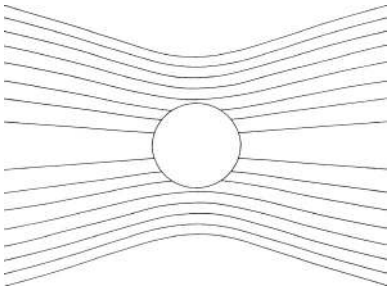

Fig. 3. Streamlines around a solid moving sphere in a liquid at rest.[2)]

$$= 4\pi R_I^2 \left[\frac{\sigma_{MS}}{2(R_I + S)}\sin^2\theta + \frac{dZ}{dt}\,\frac{\mu_S}{3}\,\frac{3}{2}\left(\frac{1}{R_I + 2S} - \frac{1}{R_I + 4S}\right)(1 - \cos^3\theta_C)\right] \quad \text{.....(16)}$$

where the following expressions for the angles are obtained from the geometry in Fig. 2 as

$$\sin^2\theta_C = \frac{(2R_I + S - Z)(S + Z)}{(R_I + S)^2} \quad \text{.....(17)}$$

$$\cos\theta_C = \frac{R_I - Z}{R_I + S} \quad \text{.....(18)}$$

Because of the accelerated liquid motion, the buoyancy force is written as

$$F_b = \frac{4}{3}\pi R_I^3 (\rho_M - \rho_I) g \quad \text{.....(19)}$$

The drag force is described by

$$F_d = 6\pi R_I \mu_M \frac{dZ}{dt} \quad \text{.....(20)}$$

The added mass force is expressed as

$$F_f = \frac{2}{3}\pi R_I^3 \rho_M \frac{d^2 Z}{dt^2} \quad \text{.....(21)}$$

The equation of motion (Eq. (2)) for the model including a steel film can now be expressed as follows for the dimensionless displacement of the inclusion

$$\frac{d^2 Z^*}{dt^{*2}} = 2\,\frac{\rho_M - \rho_I}{\rho_M + 2\rho_I} - 3G \cdot H(Z^*, S^*) - \frac{2}{J} K(Z^*, S^*)\frac{dZ^*}{dt^*} - \frac{9}{I}\frac{dZ^*}{dt^*} \quad \text{.....(22)}$$

where G, H, I, J and K are defined as

$$G = \frac{\sigma_{MS}}{R_I^2 (\rho_M + 2\rho_I) g} \quad \text{.....(23)}$$

$$H(Z^*, S^*) = \frac{(2 + S^* - Z^*)(S^* + Z^*)}{(1 + S^*)^3} \quad \text{.....(24)}$$

$$I = \frac{\sqrt{R_I^3 g}\,(\rho_M + 2\rho_I)}{\mu_M} \quad \text{.....(25)}$$

$$J = \frac{\sqrt{R_I^3 g}\,(\rho_M + 2\rho_I)}{\mu_S} \quad \text{.....(26)}$$

$$K(Z^*,S^*)=\frac{3}{2}\left(\frac{1}{1+2S^*}-\frac{1}{1+4S^*}\right)\cdot\left[1-\left(\frac{1-Z^*}{1+S^*}\right)^3\right] \quad \text{.....(27)}$$

Based on the equation for the steel flow around the inclusion (Eq. (14)) the steel film flow-out velocity is given by

$$U=-\frac{1}{r\sin\theta}\frac{d\psi}{dr}\bigg|_{r=R_I,\theta=\theta_C}=-\frac{dZ}{dt}\sin\theta_C \quad \text{.....(28)}$$

The film surface area, δ, is described as

$$\delta=\int_0^{\theta_C}2\pi R_I\sin\theta\cdot R_I d\theta=2\pi R_I^2\frac{S+Z}{R_I+S} \quad \text{.....(29)}$$

and the continuity of the film flow is expressed as

$$S\delta-U(2\pi R_I\sin\theta_C)Sdt=(S+dS)(\delta+d\delta) \quad \text{.....(30)}$$

where dS, dZ and $d\delta$ are small variations of S, Z and δ corresponding to a small time step dt. By substituting Eqs. (28) and (29) into Eq. (30) and after some rearrangement, assuming that $R_I \gg S$ and neglecting the second order of dS and dZ (since they are so small) the following expression is obtained for the dimensionless steel film thickness

$$\frac{dS^*}{dt^*}=\frac{-\dfrac{dZ^*}{dt^*}(2-Z^*)(S^*+Z^*)S^*-S^*\dfrac{dZ^*}{dt^*}}{2S^*-Z^*} \quad \text{...(31)}$$

By solving Eqs. (22) and (31) numerically, the displacement of the inclusion from the initial position and the film thickness can be calculated.

The systems of differential equations were solved using the commercial software MATLAB 6.5.

3. Characteristics of Particle Behavior across the Interface

According to the mathematical model outlined above, there are three different types of behavior that the inclusion can adopt at the interface depending on the interfacial properties of the system, the size and initial velocity of the inclusion; i) pass, ii) remain and iii) oscillate. These three modes of inclusion behavior are schematically outlined in **Fig. 4**. As mentioned before the center of the inclusion will have to be displaced one inclusion diameter from its original position in order to pass from the steel to the slag. In the so called remain case, the inclusion stays at the interface and is not completely transferred to the slag. In the oscillating case, the inclusion initially rises upwards to a maximum position from where it descends to a position slightly above the original location. From this position the inclusion rises once again. This continues for some time while the oscillations are gradually dampened out and the inclusion finally comes to rest at an equilibrium position, with the center of the inclusion located beneath the interface. It is apparent that both in the remain and in the oscillate mode the inclusion might be washed back into the steel, by a steel flow that is parallel to the interface. These two modes should therefore be avoided if an increased steel cleanliness is desired.

- **Parameter Study**

In order to elucidate which of the variables in the above model, is most influential on the calculated displacement of the inclusion, a parametric study has been performed. It is assumed that the inclusion is a spherical Al_2O_3 inclusion. This inclusion type has been chosen since this is one of the most common inclusion types. Furthermore, this type of inclusion is completely solid and undeformable at the steel making temperature (1 550°C) in the tundish, which makes it comply with the assumptions that have been made about the inclusion when outlining the model. Another reason for choosing the Al_2O_3 inclusion type for the parametric study is that it is relatively well documented in terms of high-temperature physical property data.

The parametric study was performed by first holding the Al_2O_3 inclusion diameter constant at 20 μm and then changing the diameter to 100 μm, while the physical property parameters, ρ_S, ρ_I, ρ_M, μ_S, μ_M, σ_{IS}, σ_{MI} and σ_{MS}, in the model were varied. Standard values of the physical property parameters were chosen,[3] where the steel was pure iron containing 0.005 mass% S and 0.0025 mass% O. The slag composition was chosen to be (44.1mass%)SiO_2–(6.6mass%)Al_2O_3–(4.3mass%)CaF_2–(2.6mass%)MgO–(34.6mass%)CaO–(7.8mass%)Na_2O. Each parameter in the model was then changed with −40%, −20%, +20% and +40%. Typical results from this procedure can be seen in **Fig. 5**, here exemplified by the interfacial tension between the inclusion and the steel for a 20 μm inclusion. It is ap-

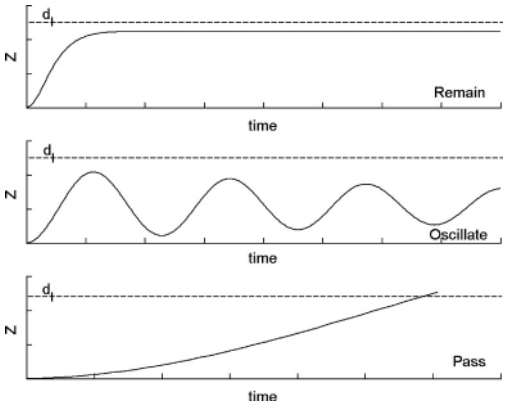

Fig. 4. The three types of behavior (remain, oscillate and pass) for the Al_2O_3 inclusion at the steel–slag interface.

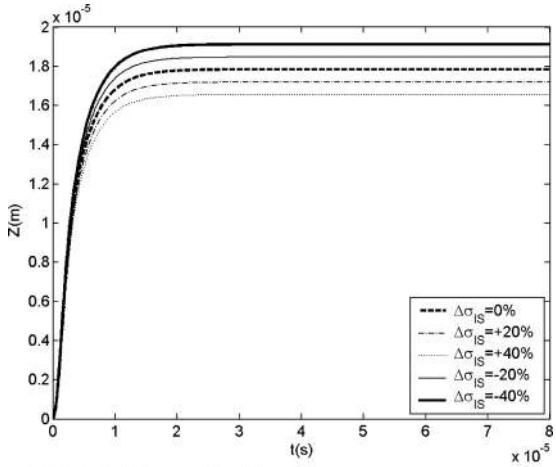

Original calculation conditions[3]

σ_{IS} (N/m)	σ_{MS} (N/m)	σ_{MI} (N/m)	ρ_M (kg/m3)	ρ_S (kg/m3)	ρ_I (kg/m3)	μ_M (Pa's)	μ_S (Pa.s)	d_I (μm)
0.440	1.375	1.518	7000	2543	3990	0.006	0.1998	20

Fig. 5. The effect of the change in the interfacial tension between the steel and an Al_2O_3 inclusion.

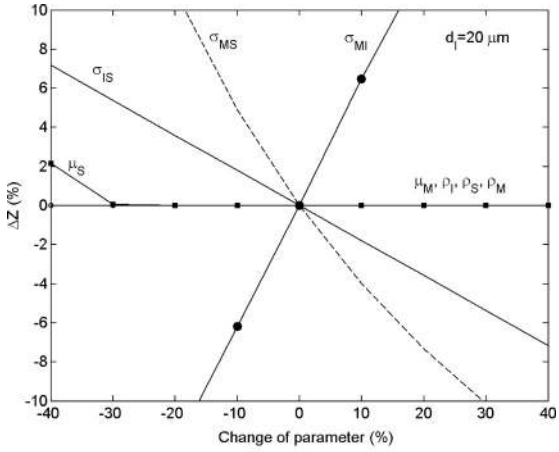

Original calculation conditions[3)]

σ_{IS} (N/m)	σ_{MS} (N/m)	σ_{MI} (N/m)	ρ_M (kg/m3)	ρ_S (kg/m3)	ρ_I (kg/m3)	μ_M (Pa's)	μ_S (Pa.s)	d_I (μm)
0.440	1.375	1.518	7000	2543	3990	0.006	0.1998	20

Fig. 6. The influence of the parameters in the inclusion transfer of a 20 μm alumina inclusion when changed by ±40%.

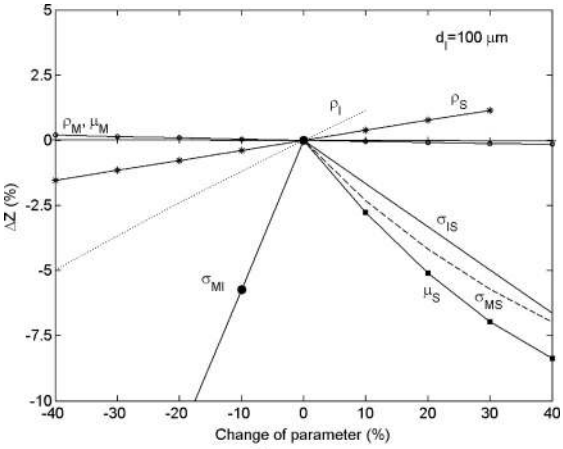

Original calculation conditions[3)]

σ_{IS} (N/m)	σ_{MS} (N/m)	σ_{MI} (N/m)	ρ_M (kg/m3)	ρ_S (kg/m3)	ρ_I (kg/m3)	μ_M (Pa's)	μ_S (Pa.s)	d_I (μm)
0.440	1.375	1.518	7000	2543	3990	0.006	0.1998	100

Fig. 7. The influence of the parameters in the inclusion transfer of a 100 μm Al_2O_3 inclusion when changed by ±40%. Note: Some of the lines are cut short due to the inclusion passing into the slag.

parent from the figure that the maximum of each curve appears at the same time which indicates that the inclusion exhibits the same type of transfer mode in all configurations of the parameter.

Curves like the ones shown in Fig. 5 were made for all of the physical property parameters in the model. Thereafter, the displacement of the inclusion, relative to the initial position, was also plotted as a function of the change of the respective parameter, which can be seen in **Fig. 6** for a 20 μm inclusion and in **Fig. 7** for a 100 μm inclusion. From these figures, it is apparent that the parameters with the greatest impact for the inclusion transfer are the interfacial tensions (σ_{IS}, σ_{MI} and σ_{MS}) together with the slag viscosity (μ_S) and for inclusions of 100 μm diameter also the inclusion density and slag density is important. Furthermore, it can be concluded from Figs. 6 and 7 that the density and the viscosity of the steel do not have any major influence on the inclusion displacement.

The slag viscosity (μ_S) and the overall wettability

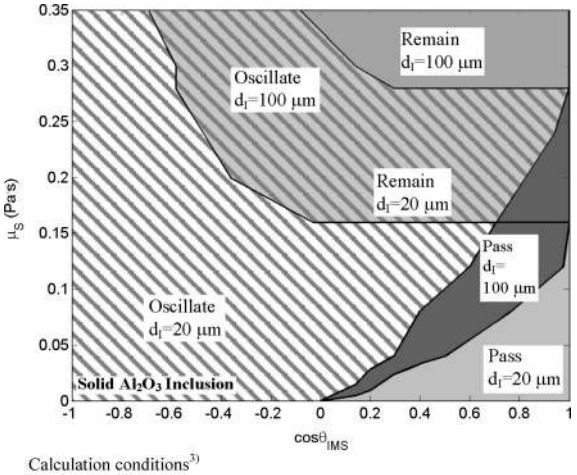

Calculation conditions[3)]

σ_{MS} (N/m)	ρ_M (kg/m3)	ρ_S (kg/m3)	ρ_I (kg/m3)	μ_M (Pa's)
1.375	7000	2543	3990	0.006

Fig. 8. The effect of the slag viscosity and the wettability, on the behavior of a solid Al_2O_3 inclusion.

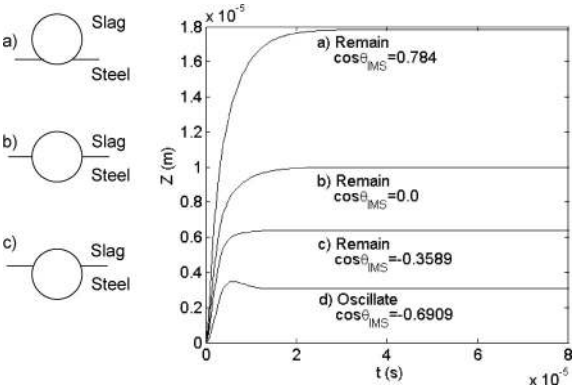

Fig. 9. Three types of remain for a 20 μm alumina inclusion as the slag viscosity and the interfacial tension between metal and slag are held constant (μ_S=0.2397 Pa·s and σ_{MS}=1.375 N/m respectively) and the overall wettability varies.

($\cos\theta_{IMS}$) were varied to see if the removal of Al_2O_3-inclusions were improved. The result is illustrated in **Fig. 8** for a 20 μm and a 100 μm solid spherical Al_2O_3 inclusion. As seen in Fig. 8, the slag viscosity and the overall wettability have to be balanced optimally in order to get the right conditions for inclusions to pass into the slag. A low slag viscosity and a high overall wettability ($\cos\theta_{IMS}>0$) are the optimal conditions for inclusion transfer. One can also see that the diameter of the inclusion has an important role in determining if the inclusion gets separated to the slag. The 100 μm inclusion has a larger region of positive conditions for passing into the slag, while the region where the inclusion remains in the steel is smaller. Furthermore, the region in which the inclusion oscillates at the steel–slag interface is larger for this inclusion size compared to the smaller size. This means that the bigger inclusion has a larger susceptibility for oscillation and is therefore also more likely to follow the steel flow back to the steel bath than the smaller one.

Three different types of "remain cases" can be identified as illustrated in **Fig. 9** for a 20 μm inclusion. Here the slag viscosity (μ_S=0.2397 Pa·s) is held constant as the overall wettability is varied. The final displacement of the inclusion from its initial position varies with the wettability. A high wettability gives the inclusion a larger final displacement

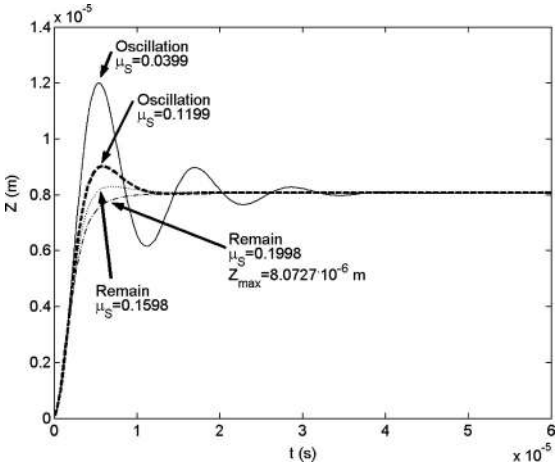

Fig. 10. Different types of oscillation for a 20 μm alumina inclusion as the overall wettability is held constant ($\cos\theta_{IMS}=-0.193$ where $\sigma_{MS}=1.375$ N/m) and the slag viscosity varies.

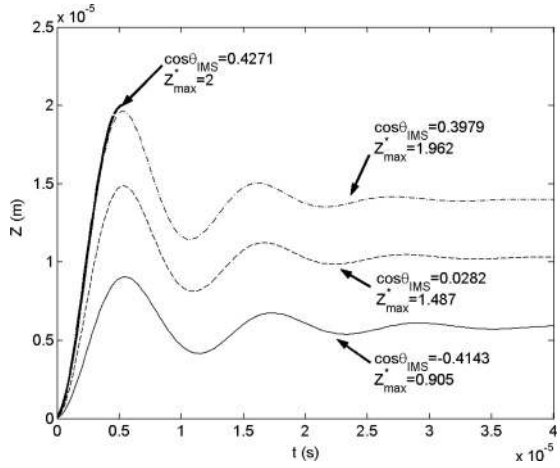

Fig. 11. A schematic figure of the change in the oscillating amplitude for a 20 μm alumina inclusion as the slag viscosity and the interfacial tension between metal and slag are held constant ($\mu_S=0.0399$ Pa·s and $\sigma_{MS}=1.375$ N/m respectively) and the overall wettability varies.

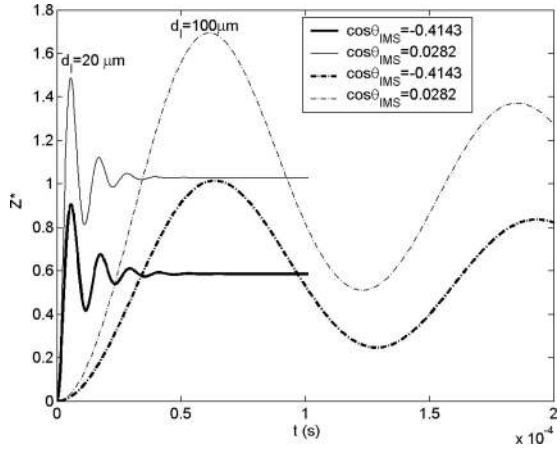

Fig. 12. The effect of inclusion size on the maximum dimensionless displacement and oscillating period as the slag viscosity is constant ($\mu_S=0.0399$ Pa·s). Note: Solid lines corresponds to $d_I=20\,\mu$m, dotted lines to $d_I=100\,\mu$m, thick lines to $\cos\theta_{IMS}=-0.4143$ and thin lines to $\cos\theta_{IMS}=0.0282$. Here $\sigma_{MS}=1.375$ N/m.

position than an inclusion where the wettability is negative. It is seen in Fig. 9 that when the overall wettability is high (a), the inclusion is almost absorbed by the slag and there is a possibility for dissolution of the inclusion to the slag. If the wettability is negative (c), the final displacement of the inclusion is smaller and most of the inclusion remains in the steel. Therefore, the possibility of entrainment of the inclusion to the steel bath is likely to happen. In the case where half of the inclusion is in the slag and half is in the steel (b), the remain case is neutral.

The shape of the oscillating curves changes also as we move from the oscillating region in Fig. 8 towards the pass and remain region. In **Fig. 10**, the change in the oscillating curves is visualized for a 20 μm Al_2O_3 inclusion as the overall wettability is held constant ($\cos\theta_{IMS}=-0.193$) and the slag viscosity is the variable parameter. It is seen that as the viscosity increases, the oscillating amplitude decreases. Also one can see that the final displacement of the inclusion from its initial position becomes the same, regardless of the oscillation amplitude and slag viscosity. Inclusion entrainment to the steel is therefore more likely to happen for slags with low viscosity and inclusions with large oscillation amplitude.

If instead, as visualized in **Fig. 11**, the slag viscosity is constant ($\mu_S=0.0399$ Pa·s) and the overall wettability ($\cos\theta_{IMS}$) increases, the amplitude of the oscillation increases. However, the shape of the curves remains the same.

In order to investigate the effect of inclusion size on the dimensionless displacement, two oscillating curves in Fig. 11 were made dimensionless and the same conditions were applied to 100 μm inclusions. The result is seen in **Fig. 12**. Solid lines corresponds to $d_I=20\,\mu$m and dotted lines to $d_I=100\,\mu$m. It is seen that not only the amplitude is larger, but also the oscillating period is longer for the 100 μm inclusion. Hence, the larger inclusions might be more susceptible to re-enter the steel bath.

Finally, it should be mentioned that the results of the parameter study showed that the model predictions were very sensitive to changes of certain physical property parameters.

4. Absorption Ability of Actual Tundish Slags

4.1. Chemical Composition of Actual Tundish Slags

Data from two different plants have been used to test the applicability of the model (Sec. 2) for separation of inclusions at the steel–slag interface. These two steel plants, one low carbon steel grade producer and one stainless steel grade producer, will in the following be designated *PLANT1* and *PLANT2* respectively. The steel plant designated *PLANT1* has a one-strand slab caster and the plant designated *PLANT2* has a three-strand billet caster. Due to the difference in the number of strands and the geometry of strands, the two steel plants have entirely different tundish geometries and sizes, which also, of course, results in different flow fields in the respective tundish. This aspect is, however outside the scope of the present study.

Typical steel compositions for the two steel plants can be seen in **Table 1** and the chemical composition of the ladle slag, tundish cover powder and tundish slags found during

Table 1. Steel composition (mass%) for the two steel plants investigated in this study.

	C	S	Mn	P	Cu	Si	Ca	Ni	B
PLANT1	0.0061	0.01	0.63	0.009	0.005	0.01	1 ppm	0.038	1 ppm
PLANT2	0.016	7 ppm	0.77	0.018	0.15	0.51	27 ppm	5.23	25 ppm
	V	Nb	Al	Ti	Cr	Sn	Mo	N	Co
PLANT1	0.004	0.001	0.053	0.001	0.013	0.001	-	46 ppm	
PLANT2	0.05	0.01	0.009	<0.005	22.09	-	3.12	0.186	0.058

Table 2. The chemical composition of the slag in the tundish of the low carbon steel plant (*PLANT1*) and the stainless steel plant (*PLANT2*).

			Slag composition (mass%)								
	Slag	Description	CaO	SiO_2	Al_2O_3	FeO	TiO_2	MnO	MgO	K_2O	State at 1823K[21]
PLANT1	Ladle	Ladle slag	36.8	6.3	31.3	8.7	0.6	8.4	6.1	0.03	Liquid
PLANT1	A1	just before first ladle change	3.4	57	27.9	6	-	-	1.8	3.9	Liquid
	A2	after first ladle change	11	47	16.2	11	-	11.5	3.2	-	Liquid
PLANT1	A3	during first ladle	1.08	93.7	1.08	0.96	-	-	1.08	2.1	Solid
	A4	after first ladle change	16.8	54	9.5	11.5	1.6	3	3.6	-	Liquid
PLANT2	B1	during first ladle	57.8	8.2	1.6	0.82	0.18	-	31.4	-	Solid
	B2	just before first ladle change	8.3	42.3	18.4	-	-	-	31	-	Liquid

casting in the two steel plants can be seen in **Table 2**.

In *PLANT1*, the ladle slag containing a lot of MnO and FeO is carried over from the ladle to the tundish. Therefore, the tundish slag A1 just before the first ladle change is a mixture of the tundish cover powder and the ladle slag and contains both FeO and MnO. Also in *PLANT1* another tundish cover powder of crude silica is used, slag A3. Because of slag carry over from the ladle into the tundish, the tundish slag in this case also is a CaO–SiO_2–Al_2O_3–FeO–MnO–MgO system.

In *PLANT1*, the tundish slag contains oxide components that easily could be reduced by for example aluminium in the steel. These chemical reactions will indeed alter the interfacial properties at the steel–slag interface. This matter will be discussed further in a subsequent section.

In *PLANT2*, a cover powder consisting of mostly CaO and MgO is used, slag B1. Because of the ladle slag carry over to the tundish pouring a ladle slag without FeO and MnO, the tundish slag B2 is a CaO–SiO_2–Al_2O_3–MgO system. It can therefore be assumed that there will be no chemical reactions between the steel and the tundish slag.

As can be seen in Table 2, slag A1, A2 and A4 for *PLANT1* together with slag B2 for *PLANT2* are fully liquid at the considered temperature. Since a fully liquid slag is one of the requirements of the mathematical model only these four slags will be considered in the application of the mathematical model described in the preceding section.

In continuous casting there is no slag when the tundish starts to be filled, but after filling up the tundish half-way a tundish cover powder is applied to the naked steel surface to cover the steel and protecting it from the surrounding air and reoxidation. During the casting of the first ladle, steel and also some ladle slag enters the tundish. This ladle slag follows the steel flow to the tundish cover powder forming a slag, which is a mixture of ladle slag and tundish cover powder. Measurements at the steel plant designated *PLANT1* using an iron thread to measure the slag thickness showed that six minutes after the casting process started the slag thickness was about 25 mm and just before ladle change it approximately 28 mm thick. After the first ladle change the slag thickness increased rapidly. At the second ladle change (1.5 h after the casting started) the slag was almost 75 mm and after the third ladle-change the slag thickness was roughly 142 mm.

To be able to apply the previously described mathematical model for inclusion transfer to the conditions found in the two steel plants investigated in this study there are some physical property parameters (ρ_S, ρ_I, ρ_M, μ_S, μ_M, σ_{IS}, σ_{MI} and σ_{MS}) that needs to be determined. As the results of the parameter study showed the effect of some of these data (σ_{IS}, σ_{MI} and σ_{MS} and μ_S) on the predictions is large. The lack of experimental data for these physical properties, applicable to systems of industrial relevance, forces us to use a number of estimating methods.

Table 3. Comparison of viscosity models for slags with[9] and without[10] FeO.

Slag composition (mass%)						Measured viscosity (Pa's)	Riboud[4] (Pa's)	Urbain[5] (Pa's)	Thermoslag[7] (Pa's)	Nakajima[6] (Pa's)
Al_2O_3	CaO	MgO	FeO	MnO	SiO_2					
18.7	40.6	3.4	0.7	-	31.1	0.425[9]	0.485	1.702	0.532	-
13.5	45.2	3.4	0.5	0.4	33.4	0.275[9]	0.309	1.355	0.383	-
15.2	38.5	5.1	1.0	0.7	36.0	0.400[9]	0.511	1.853	0.477	-
14.8	41.6	11.9	0.3	0.8	29.7	0.250[9]	0.165	0.932	0.215	-
25	30	10	-	-	35	0.5[10]	0.989	2.472	0.584	0.580
20	30	10	-	-	40	0.7[10]	1.007	2.827	0.662	0.624
25	20	10	-	-	45	1.8[10]	3.527	6.818	1.870	1.309
20	20	10	-	-	50	2.2[10]	3.496	8.758	2.31	1.393

Here, it should be noted that experimental errors or uncertainties associated with high-temperature physical property data, especially slag viscosities and interfacial tensions, very often can be found in the range ±20–40% or more. This is most likely also true for model predictions of physical properties.

4.2. Estimation of Slag Viscosity

The slag viscosity was earlier found to be one of the parameters that have the greatest influence on the predictions. Since experimental data are scarce for slag systems relevant to tundish slags, some models for prediction of slag viscosities data have been studied. More specifically, the studied models are the Riboud model,[4] the Urbain model,[5] the Nakajima model[6] and the software ThermoSlag.[7] Both the Riboud model and the Urbain model are based on an interpolation formula obtained from Arhenius plots of measured viscosity values. Thermoslag is a software program based on the absolute reaction-rate theory where the viscosity can be expressed in terms of Gibbs energy of activation. Nakajima model is based on the network parameter model by Iida.[8] In order to compare the performance of these four slag viscosity estimation methods, a "benchmark" calculation were made using a Al_2O_3–CaO–MgO–FeO–MnO–SiO_2 slag[9] and a Al_2O_3–CaO–MgO–SiO_2 slag.[10] The results of this calculation compared with experimentally measured viscosities can be seen in **Table 3**.

Since the slags for *PLANT1* consists of high amounts of FeO and MnO, the Riboud, Urbain and Thermoslag can be used to estimate the viscosity of these slags. However, Urbains method proved to be inaccurate. In this study the Riboud model has been selected for the slags containing FeO and MnO. For *PLANT2*, with no FeO in the slag, the Riboud model, Thermoslag and Nakajima model proved to be accurate. The Nakajima model was selected, due to its potential to estimate the viscosity for slags containing Li_2O, which is an oxide that reduces the slag viscosity and is therefore often found in tundish and mold fluxes.

4.3. Estimation of Molar Volume and Slag Density

Gaye introduced values for the molar volume of slags.[11] Mills and Keene developed an additive rule for the estima-

tion of densities of slags.[12] Nakajima modified it and introduced an interaction parameter into the model.[13] In Mills and Keene's method slag densities for slags including FeO, TiO_2 and MnO can be estimated. Nakajima's model however, is not valid for systems with FeO but instead it is valid for slags with Li_2O. Therefore, the Mills method was used to estimate the slag densities for the slags with FeO and Nakajima's model for slags without FeO.

4.4. Estimation of Surface Tension

Boni introduced values for the surface tension of slags.[14] Mills and Keene developed an additive rule for the estimation of slags surface tension.[15] Nakajima modified it and introduced an interaction parameter into the model.[16] The Nakajima model does not consider FeO and MnO in the slags. Therefore Mills and Keene's model is used for the slags with FeO and Nakajima's model is used for the slags without FeO. Since the slags containing FeO are extremely active against the steel containing aluminum, reoxidation occurs. This violates with the assumption in the model that no chemical reactions at the interface is allowed to occur and the surface tension of the metal will drop rapidly.

4.5. Estimation of Interfacial Tension

Girifalco and Good[17] developed a model for the estimation of interfacial tension data relevant for two combined water-organic phases. The interfacial surface tension could be expressed as

$$\sigma_{ab} = \sigma_a + \sigma_b - 2\phi\sqrt{\sigma_a \cdot \sigma_b} \quad \text{.....(32)}$$

where σ_a and σ_b is the interfacial tensions for phases *a* and *b* respectively and ϕ is an interaction coefficient describing the interaction between *a* and *b*. Nakajima's model for slags and steel,[18] is based on the work done by Girifalco and Good. The interaction coefficient ϕ tends to zero when there is a weak attraction between the phases and to unity when the attraction between the two phases is strong. It is calculated backwards as a function of slag chemistry from already measured interfacial tensions. In this work, the Nakajima approach with selected literature data have been used to estimate the interfacial tension between inclusion and slag, inclusion and steel as well as slag and steel. In the estimations of the interaction parameters between slag and steel and between slag and inclusion, the FeO and MnO content in the slags have been neglected.

5. Results and Discussion

After determining the physical properties for the four slags that were determined to be fully liquid (A1, A2 and A4 in the case of *PLANT1* and B2 in the case of *PLANT2*), see **Table 4**, the displacement of the inclusion from its original position was calculated. The results are plotted in **Fig. 13**. In this figure, the slag viscosity is plotted as a function of the overall wettability. The changes from remain to pass, from pass to oscillate and from remain to oscillate are in the same figure plotted for a 20 μm inclusion and a 100 μm inclusion. Because the slags A1, A2 and A4 contains FeO and are highly reactive with the steel, the surface tension of the metal decreases rapidly during the reoxidation process leading to a rapid drop in the interfacial tensions between metal–slag and inclusion-metal. Therefore, an error bar is included for these slags in Fig. 13. The interfacial tension changes in time and after the reactions have stopped, the interfacial tension will increase again. However, the slag composition and metal composition will have changed and

Table 4. Rough estimation of physical properties for the two steel plants (*PLANT1* and *PLANT2*).

	Slag A1	Slag A2	Slag A4	Slag B2
μ_S (Pa·s)	24.59[4]	1.987[4]	2.360[4]	0.407[6]
ρ_S (kg/m^3)	3801[12]	3330[12]	3557[12]	2585[13]
σ_S (N/m)	0.309[12]	0.420[12]	0.399[12]	0.403[16]
ϕ_{IS}[16]	0.232*	0.431*	0.480*	0.644
ϕ_{MS}[16]	0.511*	0.442*	0.419*	0.301
σ_{IS} (N/m)[16]	0.835	0.686	0.624	0.445
σ_{MS} (N/m)[16]	1.241	1.346	1.381	1.760
σ_{MI} (N/m)[16]	1.561	1.561	1.561	1.724
$\cos\theta_{IMS}$	0.584	0.650	0.679	0.727

* Neglects FeO, MnO and TiO_2 content in the estimation of ϕ_{IS} and ϕ_{MS}.

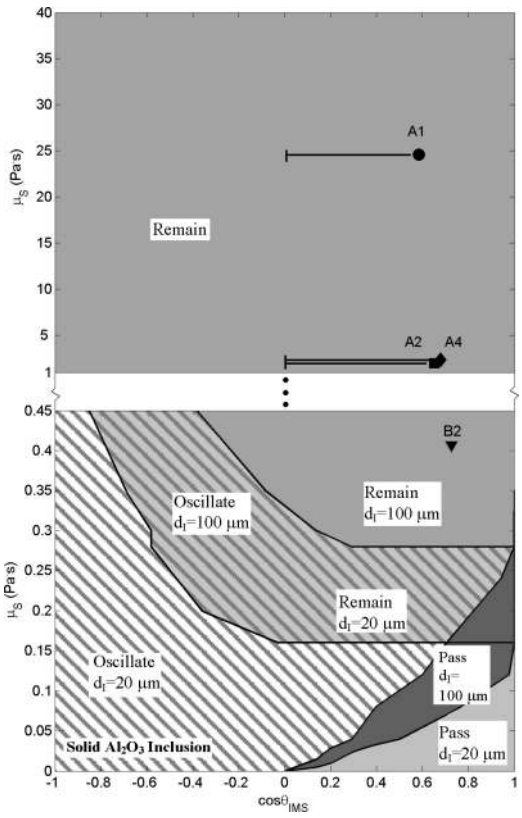

Fig. 13. Estimation relationship between the slag viscosity and wettability for the conditions in *PLANT1* and *PLANT2*. Here the interfacial tension between metal and slag is constant, σ_{MS}=1.375 N/m.

the interfacial tension will not have the same original value anymore. This phenomena has been studied and reported by, for example amongst others, Riboud and Lucas.[19]

The overall conclusion about the application of the model to industrial cases is that very meaningful plots can be made, which shows how the tendency for inclusion transfer across the steel–slag interface can be visualized. Furthermore, these plots can show how the slag viscosity and wettability needs to be adjusted for the specific slags in order to increase the chances for inclusions of different sizes to be separated to the slag (reach the pass region).

The data for the slags A1, A2, A4 and B2 shows that both a 20 μm and a 100 μm inclusion will most likely remain in the steel. In order for these sizes of inclusions to reach a pass situation and thereby being separated to the slag, the slag viscosity must be decreased and the wettability must be increased.

5.1. Suggestions for Slag Improvement

In order to make the solid Al_2O_3 inclusions separate to the slags in *PLANT1* and *PLANT2*, the slags needs to be modified. First of all, if *PLANT1* is going to get better con-

Table 5. Chemical composition of two slags with lower viscosity.

Slag	CaO (mass%)	SiO_2 (mass%)	Al_2O_3 (mass%)	MgO (mass%)	Li_2O (mass%)	μ_S (Pa's)	σ_S (N/m)	ρ_S (kg/m^3)
1	40	30	10	20	-	0.072	0.523	2728
2	40	40	10	-	10	0.087	0.468	2470

Table 6. The effect on slag viscosity and overall wettability when changing Slag 1 and Slag 2 applied to *PLANT1*.

Slag	$\frac{CaO}{SiO_2}$	$\frac{Al_2O_3}{MgO}$	$\frac{Al_2O_3}{Li_2O}$	μ_S	$\cos\theta_{IMS}$	Comments
1	1.3	0.5		0.072	0.813	σ_{MI}=1.561 N/m
	-	↑		↑	↓	
	-	↓		↓	↓	
	↑	-		↓	↑	Solid at 1873K
	↓	-		↑	↓	
	↑	↓		↓	↑	Solid at 1873K
	↓	↑		↑	↓	
2	1		1	0.087	0.631	σ_{MI}=1.561 N/m
	-		↑	↑	↑	
	-		↓	↓	↓	
	↑		-	↓	↑	Risk for slag entrainment
	↓		-	↑	↓	
	↑		↓	↑	↓	
	↓		↑	↑	↑	

- original value
↑ parameter increases
↓ parameter decreases

Table 7. The interfacial tensions and overall wettability for the new slags applied to the conditions in *PLANT1* and *PLANT2*.

	Slag	σ_{IS} (N/m)	σ_{MS} (N/m)	σ_{MI} (N/m)	$\cos\theta_{IMS}$
PLANT1	1	0.388	1.442	1.561	0.813
	2	0.631	1.474	1.561	0.631
PLANT2	1	0.388	1.612	1.724	0.828
	2	0.631	1.649	1.724	0.662

ditions in the tundish the FeO and MnO in the ladle slag has to be removed and/or the extensive ladle slag carry over to the tundish has to be drastically reduced. Secondly, the viscosity as well as the liquid temperature of the slag has to decrease, which is also the case for *PLANT2*.

This can be accomplished by creating a slag where:

1) $\frac{\text{wt\%CaO}}{\text{wt\%SiO}_2} \approx 0.8$–$1.3$ in order to have a liquid slag at 1 550°C
2) mass%$Al_2O_3 \approx$10–15 to get good wettability of Al_2O_3 inclusions
3) Addition of MgO or Li_2O to reduce the viscosity

Table 5 shows two slag systems, CaO–SiO_2–Al_2O_3–MgO (Slag 1) and CaO–SiO_2–Al_2O_3–Li_2O (Slag 2), with low slag viscosity and a liquid temperature at 1 450°C. **Table 6**, shows what happens to the slag viscosity and the overall wettability if the amount of each component in Slag 1 and Slag 2 changes when applied to *PLANT1*. It can for example be seen that when the basicity (CaO/SiO_2) increases, the slag viscosity decreases and the overall wettability increases. The opposite occurs if the basicity decreases. Applying these slags to the industrial conditions, a high overall wettability is obtained. In **Table 7**, the interfacial tensions and the overall wettability are summarized for the two steel plants. The new conditions were plotted in **Fig. 14** for *PLANT1* (designated ● and ○) and *PLANT2* (designated ◆ and ◇). It can be seen that with these new slags the 100 μm Al_2O_3 inclusions would pass for both slags. However, it is only for Slag 1 that also the 20 μm Al_2O_3 inclusions gets

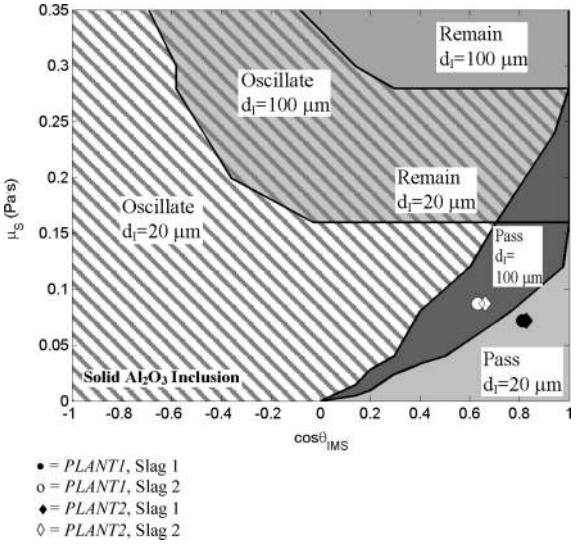

● = *PLANT1*, Slag 1
○ = *PLANT1*, Slag 2
◆ = *PLANT2*, Slag 1
◇ = *PLANT2*, Slag 2

Fig. 14. Estimation relationship between the slag viscosity and wettability for the new slags applied to the conditions in *PLANT1* and *PLANT2*. Here the interfacial tension between metal and slag is constant, σ_{MS}=1.375 N/m.

separated. Therefore, for the separation of inclusions to the slag the recommendation for the industry would be to modify their slags towards the composition of Slag 1.

5.2. Other Solid Inclusions

Solid inclusions with compositions other than pure alumina are frequently found during the processing of liquid steel. Therefore, a similar study as in Sec. 3.1 was made on a solid Al_2O_3–MgO (90/10 mass%) inclusion and a solid Al_2O_3–CaO (85/15 mass%) inclusion to investigate changes in the areas of inclusion behavior. The result can be seen in **Fig. 15**. It should be noted that the inclusion densities were determined by an additive rule, where the density of each inclusion component were multiplied by the molar fraction of that component. In Fig. 15, it is seen that the pass regions for 20 μm and 100 μm inclusions and the remain region for 20 μm inclusions are the same. It can also be seen that the remain area for the 100 μm inclusions is changing a little depending on inclusion composition. However, the inclusion compositions are mostly Al_2O_3, so the effect might therefore had been more noticeable if the inclusions had contained some other element than Al_2O_3. Furthermore, from the parameter study it was concluded that for 100 μm inclusions the slag and inclusion density started to affect the inclusion behavior. Since the slag density is the same for all three inclusions in this case, perhaps it is possible that the inclusion density is affecting the lines for the oscillating and remain regions causing a shift in the lines. Finally, the crossing of the lines for the 100 μm inclusions in the remain region could be due to different interfacial tension between metal and inclusion.

6. Conclusions

A mathematical model has been used to predict how inclusions are transferred across a steel–slag interface. The inclusion can behave in three ways as it reaches the steel–slag interface. It can pass and enter the slag almost instantaneously, remain at the interface where it may act as a build up place for clusters that can re-enter the steel bath with the steel flow and cause nozzle clogging in the end, or oscillate and follow the flow to the steel causing product

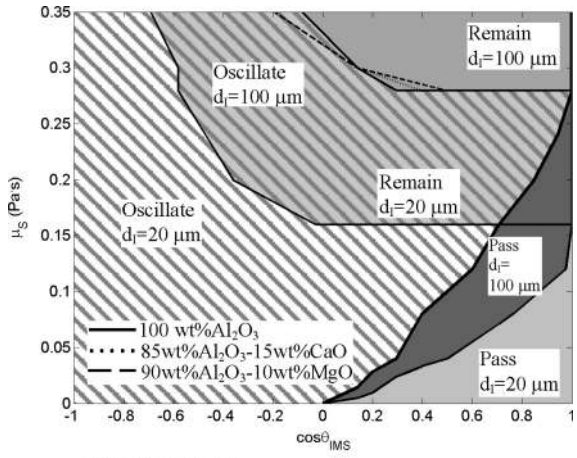

Calculation conditions

Inclusion	σ_{MS} [3] (N/m)	σ_{MI} (N/m)	ρ_M [3] (kg/m3)	ρ_S [3] (kg/m3)	ρ_I (kg/m3)	μ_M [3] (Pa's)
Al_2O_3 (100 mass%)	1.375	1.518 [3]	7000	2543	3990 [3]	0.006
Al_2O_3-MgO (90/10 mass%)	1.375	1.417 [20]	7000	2543	3912	0.006
Al_2O_3-CaO (85/15 mass%)	1.375	1.327 [20]	7000	2543	3840	0.006

Fig. 15. Estimation of the relationship between overall wettability and slag viscosity for solid Al_2O_3 inclusion, solid Al_2O_3–MgO inclusion (90/10 mass%) and solid Al_2O_3–CaO inclusion (85/15 mass%).

defects. There also exists two situations when an inclusion passes the interface, one in which a steel film is formed between the inclusion and the slag and another where no steel film is formed. However, it has been concluded in this work that the steel film formation occurs when the inclusion diameter is roughly 150 μm. Since most non-metallic inclusion found in modern steel grades in a tundish are far smaller than that diameter, the non-film case of the model is most relevant to use.

The main conclusion of this work is that the proposed mathematical model can be used to predict and to determine the critical parameters governing the separation of non-metallic inclusions at the interface between the steel and the slag. The most important parameters on the inclusion transfer have been found to be the interfacial tensions (σ_{MI}, σ_{IS}, σ_{MS}) and the slag viscosity (μS) for a 20 μm inclusion. In the case of a 100 μm inclusion also the slag and inclusion density plays a role. The combined effect of these parameters showed that the overall wettability should be positive and that the slag viscosity should be as low as possible, without creating conditions for slag entrainment to the steel, for most favorable inclusion transfer conditions. It should also be noted that data for these physical properties are also the most difficult to find in the literature. Thus, future measurements will therefore be needed in order to make predictions of inclusion transfer behavior at the steel–slag interface which are more relevant for the industry.

The model was also applied to four slag compositions originating from samples taken from the tundish at two different steel plants. Since the compositions of the slags and tundish cover powders used in *PLANT1* and *PLANT2* never have been studied experimentally before, no experimental data for the interfacial surface tensions and slag viscosities were found. These had to be estimated using available models for prediction of physical properties. The overall conclusion is that the application of the model related to industrial cases gives very useful plots, which shows the tendency for inclusion transfer across the steel–slag interface. Furthermore, it can be illustrated how the slag viscosity and the wettability need to be changed in order to increase the separation of the inclusions to the slag.

Acknowledgements

The Swedish Steel Producers Association and STEM are acknowledged for financing this work. Furthermore, I would like to appreciate the helpful comments from the members of the committee JK24046 throughout this work.

Nomenclature

g: Gravity (m/s^2)
t: Time (s)
t^*: Dimensionless time (−)
Z: Displacement of the inclusion (m)
$Z(0)$: Initial position of the inclusion (m)
S: Steel film thickness (m)
$S(0)$ Initial steel film thickness (m)
u: Terminal/initial velocity of the inclusion at t=0 (m/s)
R_I: Radius of the inclusion (m)
D_I: Diameter of the inclusion (m)

$\mathrm{Re} = \dfrac{\rho_M u_\infty D_I}{\mu_M}$: Reynolds number (−)

Greek symbols
ρ_x: Density (kg/m^3)
σ_x: Surface tension (N/m)
σ_{xy}: Interfacial tension (N/m)
μ_x: Viscosity (Pa·s)

Subscripts
S: Slag
I: Inclusion
M: Metal

Superscript
* Dimensionless

REFERENCES

1) K. Nakajima and K. Okamura: Proc. of 4th Int. Conf. on Molten Slags and Fluxes, ISIJ, Tokyo, (1992), 505.
2) R. Clift, J. R. Grace and M. E. Weber, Bubbles, Drops and Particles, Academic Press INC., New York, (1978), 34.
3) K. Nakajima: Ph.D. Thesis, Osaka University, Osaka, (1993).
4) P. Riboud, Y. Roux, L-D. Lucas and H. Gaye: *Fachber. Hüttenprax. Metallwiterverarb.*, **19** (1981), 59.
5) G. Urbain, F. Cambier, M. Deletter and M. R. Anseau: *Trans. J. Br. Ceram. Soc.*, **80** (1981), No. 4, 139.
6) K. Nakajima, H. Mizukami, M. Kawamoto and Z. Morita: *Tetsu-to-Hagané*, **80** (1994), No. 7, 509.
7) S. Seetharaman, D. Sichen and J. Y. Zhang: *J. Met.*, **51** (1999), 38.
8) T. Iida, H. Sakai, Y. Kita and K. Shigeno: *ISIJ Int.*, **40** (2000), Supplement, S110.
9) T. Koshida, T. Ogasawara and H. Kishidaka: Slag Atlas, 2nd ed., Verlag Stahleisen GmbH, Düsseldorf, (1995), 389.
10) K. C. Mills: Slag Atlas, 2nd ed., Verlag Stahleisen GmbH, Düsseldorf, (1995), 381.
11) H. Gaye, D. Lucas, M. Olette and P. V. Riboud: *Can. Metall. Q.*, **23** (1984), 179.
12) K. C. Mills and B. J. Keene: *Int. Mater. Rev.*, **32** (1987), 1.
13) K. Nakajima: *Tetsu-to-Hagané*, **80** (1994), No. 8, 593.
14) R. E. Boni and G. Derge: *J. Met.*, **8** (1956), 53.
15) K. C. Mills and B. J. Keene: *Int. Mater. Rev.*, **32** (1987), 1.
16) K. Nakajima: *Tetsu-to-Hagané*, **80** (1994), No. 8, 599.
17) L. A. Girifalco and R. J. Good: *J. Phys. Chem.*, **61** (1957), 904.
18) K. Nakajima: *Tetsu-to-Hagané*, **80** (1994), No. 5, 383.
19) P. V. Riboud and L. D. Lucas: *Can. Metall. Q.*, **20** (1981), No. 2, 199.
20) N. Shinozaki, N. Echida, K. Mukai, Y. Takahashi and Y. Tanaka: *Tetsu-to-Hagané*, **80** (1994), No. 10, 14.
21) J. O. Andersson, T. Helander, L. Höglund, P. Shi and B. Sundman: *Calphad*, **26** (2002), 273.